



OPEN

Metal-insulator transition effect on Graphene/VO₂ heterostructure via temperature-dependent Raman spectroscopy and resistivity measurement

Kittitat Lertraikul¹, Wirunchana Rattanasakuldilok², Teerachote Pakornchote¹, Thiti Bovornratanaraks¹, Illias Klanurak¹, Thiti Taychatanapat¹, Ladda Srathongsian³, Chaowaphat Seriwatanachai³, Pongsakorn Kanjanaboos³, Sojiphong Chatraphorn¹ & Salinporn Kittiwatanakul¹✉

High-quality VO₂ films were fabricated on top of *c*-Al₂O₃ substrates using Reactive Bias Target Ion Beam Deposition (RBTIBD) and the studies of graphene/VO₂ heterostructure were conducted. Graphene layers were placed on top of ~50 and ~100 nm VO₂. The graphene layers were introduced using mechanical exfoliate and CVD graphene wet-transfer method to prevent the worsening crystallinity of VO₂, to avoid the strain effect from lattice mismatch and to study how VO₂ can affect the graphene layer. Slight increases in graphene/VO₂ T_{MIT} compared to pure VO₂ by ~1.9 °C and ~3.8 °C for CVD graphene on 100 and 50 nm VO₂, respectively, were observed in temperature-dependent resistivity measurements. As the strain effect from lattice mismatch was minimized in our samples, the increase in T_{MIT} may originate from a large difference in the thermal conductivity between graphene and VO₂. Temperature-dependent Raman spectroscopy measurements were also performed on all samples, and the G-peak splitting into two peaks, G⁺ and G⁻, were observed on graphene/VO₂ (100 nm) samples. The G-peak splitting is a reversible process and may originates from in-plane asymmetric tensile strain applied under the graphene layer due to the VO₂ phase transition mechanism. The 2D-peak measurements also show large blue-shifts around 13 cm⁻¹ at room temperature and slightly red-shifts trend as temperature increases for 100 nm VO₂ samples. Other electronic interactions between graphene and VO₂ are expected as evidenced by 2D-peak characteristic observed in Raman measurements. These findings may provide a better understanding of graphene/VO₂ and introduce some new applications that utilize the controllable structural properties of graphene via the VO₂ phase transition.

Vanadium dioxide (VO₂) has attracted considerable attention from many researchers due to its Metal-Insulator Transition (MIT) effect at the transition temperature (T_{MIT}) about 68 °C under atmospheric pressure^{1,2}. As temperature rises to the T_{MIT}, VO₂ features a significant change in its electrical conductivity from non-conductive material at low temperature to conductive material at high temperature by 3 orders of magnitude, along with a considerable change in its optical transmittance and reflectance^{3,4}. The crystal structure of VO₂ also changes from monoclinic (M) phase to rutile (R) phase as the rising temperature reaches the structural phase transition temperature (T_{SPT}) which is around T_{MIT} in the pristine VO₂ condition. The contrast between VO₂ properties in these two main phases leads to various applications based on VO₂ material, such as smart windows⁵ and electrical switch^{6,7}. Various techniques were also studied in order to modify the properties related to the phase transition of VO₂ such as refining the fabrication process^{8,9}, substrate clamping^{10,11} and elemental doping^{11,12} which expand the area of its applications further. Several studies utilize the benefits of graphene, a flexible 2D material with

¹Department of Physics, Faculty of Science, Chulalongkorn University, Bangkok 10330, Thailand. ²Department of Physics, Accelerator Laboratory, University of Jyväskylä, P.O. Box 35(YFL), 40014 Jyväskylä, Finland. ³School of Materials Science and Innovation, Faculty of Science, Mahidol University, Nakhon Pathom 73170, Thailand. ✉email: salinporn.k@chula.ac.th

exceptional properties, such as high light transmittance¹³ and high electron mobility¹⁴, to improve and introduce new applications for VO₂/graphene heterostructure. Several studies report that graphene can improve VO₂ characteristic by providing higher light transmission and lower phase transition temperature^{15,16}. For the application, one of the interesting topics is the flexible thermochromic windows based on VO₂/graphene proposed by Kim et al.¹⁷. Their result indicates that graphene is a key element that allows VO₂ to adhere to the flexible substrate, poly(ethyleneterephthalate) (PET) film, thus expanding its smart windows application. Graphene layer in VO₂/graphene can also be utilized in other applications, such as changing volatile to non-volatile VO₂ transition¹⁸ and switchable terahertz absorber¹⁹. There are several previous studies about the effect between the graphene and VO₂ layers, such as the observation of thermochromism and decreases in T_{MIT} induced by electron transfer in VO₂-graphene-Ge heterostructure¹⁶ and the improvement of phase transition characteristics and optical response of VO₂ with graphene-supported layers¹⁵. However, most works were studied by fabricating VO₂ layer on top of graphene, which may lead to some limitations. Firstly, the growth process of VO₂ requires very high temperature, which can decrease the graphene layer quality, resulting in the worsening and occurrence of poly-crystalline VO₂¹⁷. Secondly, fabricating VO₂ on top of graphene could induce a compressive strain on the VO₂ originated from the lattice mismatch between graphene and VO₂. The induced strain may affect the VO₂ phase transition related properties such as the T_{MIT}. Therefore, to minimize the strain induced effect by lattice mismatch, to avoid the worsened quality of VO₂, and to probe the effect of VO₂ on graphene layer during the phase transition, the studies of graphene/VO₂ heterostructure in this work were conducted by transferring graphene layers on top of high-quality VO₂ layers fabricated on sapphire substrates instead. This work focus on probing the graphene/VO₂ crystal structure and electrical properties during the phase transition of VO₂ via temperature-dependent Raman spectroscopy and resistivity measurement, respectively. Slight increases in T_{MIT} of VO₂ with graphene layer on top were observed. The G-peak splitting, which is a reversible process, at temperature near T_{MIT} of VO₂ and higher was also observed and reported in this work for the first time, along with the unusual 2D-peak characteristics of graphene on VO₂. Raman spectra of VO₂ are also measured to probe the structural changes of the heterostructure. The results from the temperature-dependent of VO₂ peak intensity are discussed and compared to the temperature-dependent resistivity measurement, while VO₂ peak shift with the change in temperature results are included in the supplementary material. Our findings expand the knowledge about the mechanism of the graphene/VO₂ heterostructure and may be useful for future applications, such as flexible thermochromic windows and the applications that requires a controllable structural graphene properties via temperature with the help of the VO₂ phase transition.

Results and discussion

The 50 and 100 nm VO₂ thin films crystallinity and morphology were extracted using out-of-plane X-ray diffractometry (XRD) and atomic force microscopy (AFM), both results for the 100 nm VO₂ film can be seen in Fig. 1a,b, respectively (the result for 50 nm VO₂ can be found in supplementary material). The VO₂ films possess single-crystalline structures. Two XRD peaks in Fig. 1a belong to VO₂ (020) and *c*-Al₂O₃ (0006). The grain

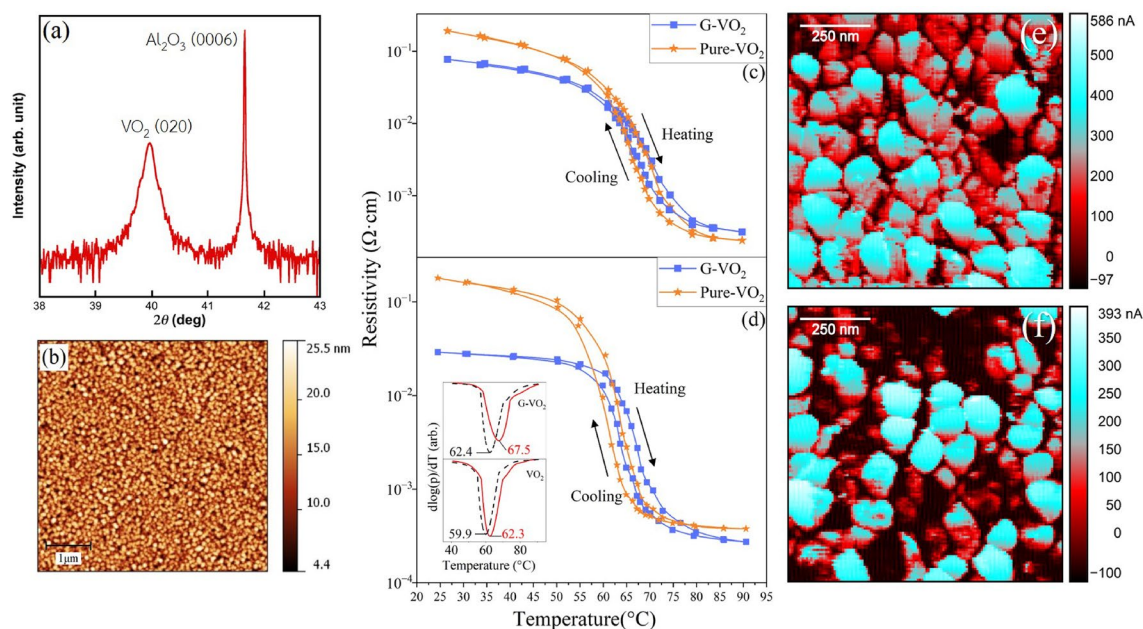


Figure 1. (a) Out-of-plane XRD scan and (b) $5 \times 5 \mu\text{m}^2$ AFM surface scan of 100 nm VO₂/*c*-Al₂O₃, respectively. The XRD and AFM scan results for 50 nm VO₂/*c*-Al₂O₃ can be found in the supplementary material. The temperature-dependent resistance measurement result of CVD-graphene/VO₂ samples with (c) 100 nm VO₂ and (d) 50 nm VO₂ (with $\frac{d(\log(\rho))}{dT}$ curve inset showing the T_{MIT} extracted from each cycle/sample area). C-AFM measurement results of CVD-graphene/VO₂ (100 nm) sample on (e) graphene area and (f) pure-VO₂ area.

distribution of VO₂ can be seen from the $\sim 5 \times 5 \mu\text{m}^2$ AFM image in Fig. 1b. The rms roughness of 100 nm VO₂ is 2.6 nm. There are no pinholes or cracks on the surface for both 50 nm and 100 nm thin films. More XRD and AFM results for the 50 nm thin film can be seen in the supplementary materials. After confirmation of the crystallinity of VO₂ films, graphene layers were transferred on top of the VO₂ films, providing 6 samples in total (including the reference samples). A1 (CVD ref) and A2 (exf. ref) are graphene/*c*-Al₂O₃ reference samples from CVD growth and mechanical exfoliation, respectively. A3 (CVD/100) and A4 (CVD/50) are graphene(CVD)/VO₂/*c*-Al₂O₃ with 100 nm and 50 nm VO₂, respectively. A5 (exf./100) and A6 (exf./50) are graphene(exfoliated)/VO₂/*c*-Al₂O₃ with 100 nm and 50 nm VO₂, respectively. Note that A3–A6 samples have both pure-VO₂ area and graphene/VO₂ area available for Raman and resistivity measurements.

Temperature-dependent resistivity measurement

The temperature-dependent resistivity on the samples A3 (CVD/100) and A4 (CVD/50) were measured in-plane and plotted in Fig. 1c,d, respectively. Both measurements include graphene/VO₂ and pure VO₂ area. There are several noticeable features in the results. Firstly, the resistivity dropped at the initial of the measurement (before the transition) for graphene/VO₂ around ~ 3 times compared to pure VO₂, which may be attributed to the fact that graphene conductivity is much higher than the VO₂ in the insulating phase²⁰, hence the in-plane resistivity measurement is simply measuring the parallel two-resistor model, resulting in lower equivalent resistance. The conductive atomic force microscopy (C-AFM) current mapping results at room temperature in Fig. 1e (graphene area) and f (pure-VO₂ area) from sample A3 (CVD/100) also confirm that graphene can improve the overall conductivity of the sample. It could also be the effect of electron injection into the VO₂ layer due to the proximity of graphene, as reported by Zhou et al.¹⁶. Secondly, the phase transitions are less sharp on G-VO₂ area compared to pure-VO₂ area. Thirdly, the T_{MIT} is slightly higher for graphene/VO₂ compared to pure VO₂. The T_{MIT} from each sample was calculated by averaging the transition temperature in the heating and cooling cycles using the following equation:

$$T_{MIT} = \frac{T_{heating} + T_{cooling}}{2} \quad (1)$$

where T_{heating} (cooling) are the critical phase transition temperature calculated by finding the minimum value of $\frac{d(\log(\rho))}{dT}$ in heating (cooling) cycle. The T_{MIT} extracted from sample A3 (CVD/100) (Fig. 1c) for graphene/VO₂ and pure VO₂ area are 69.3 °C and 67.4 °C, respectively. The T_{MIT} extracted from sample A4 (CVD/50) (Fig. 1d) for graphene/VO₂ and pure VO₂ area are 64.9 °C and 61.1 °C, respectively. The $\frac{d(\log(\rho))}{dT}$ plot of sample A3 is shown in Fig. S3a and the plot of sample A4 is shown in the inset of Fig. 1d and S3b. In general, T_{MIT} from 50 nm VO₂ sample is less than 100 nm VO₂ sample because thinner VO₂ film is subjected to higher compressive strain in *c_R* direction from VO₂-*c*-Al₂O₃ lattice mismatch, which has been reported to affect the T_{MIT}²¹. In contradiction to previous works done by Kim et al.¹⁵ and Zhou et al.¹⁶, the proximity of graphene results in higher T_{MIT} of VO₂ in our work. According to the work from Kim et al., T_{MIT} can be reduced with the presence of graphene support layer underneath¹⁵. And the more graphene layers, the lower T_{MIT} observed in VO₂¹⁵. It was proposed that the thermal expansion mismatch of the heterostructure may induce compressive strain in *c_R* (in-plane) direction. The thermal expansion coefficient (α) of graphene is known to be negative around $-3.26 \times 10^6 \text{K}^{-1}$ ²² and the α of VO₂ are known to be positive. Therefore, the mismatch between α can induce the compressive strain in VO₂. Another possible reason for lower T_{MIT} is the compressive strain on VO₂ induced by lattice mismatch between graphene and VO₂ in the growth process. With the reverse layer ordering presented in our work, the latter effect can be diminished. Another work from Zhou et al.¹⁶ proposed that the electron injection from graphene can occur between the graphene/VO₂ interface, which destabilizes the insulator phase of VO₂ and decreases T_{MIT}. This phenomenon was observed in VO₂/graphene/Ge heterostructure and described that the different in Fermi levels, which are Ge > graphene > VO₂, introduce the Schottky barrier at each interface, resulting in electron flow from Ge to graphene and from graphene to VO₂. Since the decrease in T_{MIT} cannot be observed in this work, it may indicate that the electron donor layer, such as Ge, is required for such an effect to occur. Also, it is noteworthy that the measurement technique for extracting the T_{MIT} may affect the T_{MIT} itself. Zhou also proposed that the measurement technique involving light radiation may introduce a higher carrier density, destabilize the insulator phase, and affect T_{MIT} even more. As for the increase in T_{MIT} observed in our work, due to the fact that the in-plane thermal conductivity of the graphene on Si substrate is about 500–1000 Wm⁻¹K⁻¹²³ and VO₂ is about 3–6 Wm⁻¹K⁻¹²⁴, the graphene upper layer may act as a heat sink to the VO₂ film, which can dissipate the heat out of the film. That resulted in a higher temperature required for the film to reach the actual T_{MIT} of VO₂. As seen in Fig. 1c,d, the effect of graphene on the rise of T_{MIT} is more pronounced in the thinner VO₂ film. The T_{MIT} of VO₂ is increased by 1.9 °C for sample A3 (CVD/100) and 3.8 °C for sample A4 (CVD/50). This supports the hypothesis that the heat may be dissipated via the graphene layer, and the thinner VO₂ layer, the higher heat dissipation efficiency, resulting in a larger decrease in T_{MIT}.

Temperature-dependent Raman spectroscopy

The temperature-dependent Raman spectra of 100 nm VO₂/*c*-Al₂O₃ film were measured as shown in Fig. 2a. At low temperature, the Raman spectra show the signature of VO₂ monoclinic phase including 195, 225, 616 cm⁻¹ vibrational modes. 195 and 225 cm⁻¹ modes relate to V–V vibrational modes, while $\sim 616 \text{cm}^{-1}$ mode relates to V–O vibrational mode.²⁵ As the temperature increases, all VO₂ Raman peaks intensity starts decreasing at $\sim 55 \text{°C}$ and completely disappears at $\sim 75 \text{°C}$, confirming the structural transition from monoclinic to rutile since the rutile phase is Raman inactive. VO₂ samples were cut into $\sim 1 \times 1 \text{cm}^2$ and graphene layers were transferred on top of *c*-Al₂O₃ and VO₂/*c*-Al₂O₃ samples using two techniques as described in the methods section.

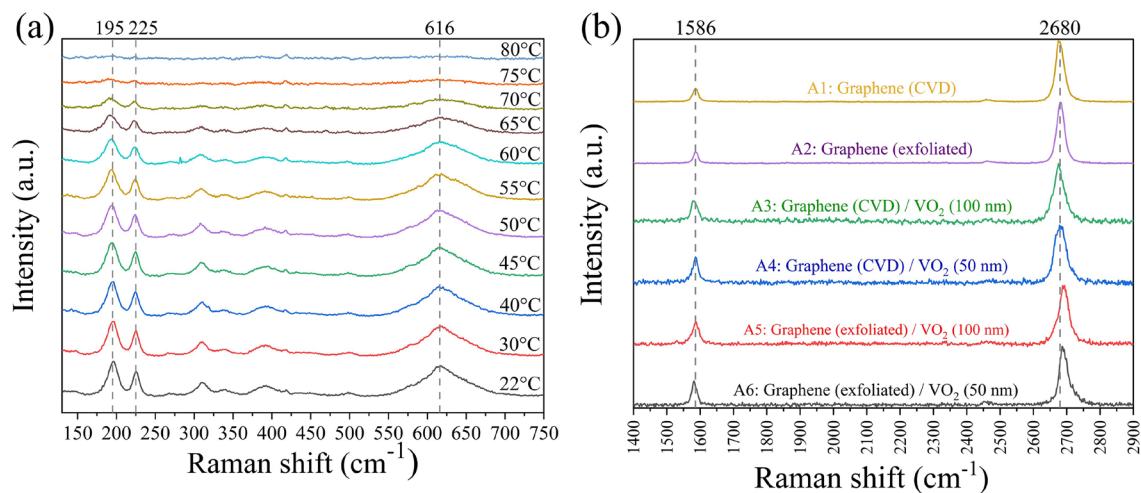


Figure 2. (a) Temperature-dependent Raman spectra of VO₂ sample, the Raman intensity of VO₂ decreases as temperature increases, and the VO₂ peaks completely disappear as temperature reaches ~70 °C (b) Raman spectra of all graphene samples on VO₂/c-Al₂O₃ substrate, the reference samples are samples A1 (CVD ref) and A2 (exf. ref).

Raman spectra of all samples (A1–A6) in graphene region are shown in Fig. 2b. The G and 2D peaks of each graphene are located at 1582–1595 cm⁻¹ and 2676–2695 cm⁻¹, respectively. The D-peaks at ~1350 cm⁻¹ of all samples are almost invisible, which indicates their good quality²⁶. Figure 3a shows the relationship between G-peak position and temperature. The initial G-peak positions for each sample at room temperature (~22 °C) are spatially dependent due to the local strain and defects on VO₂ and graphene itself, which are unavoidable. The trends of G-peak shift, however, should be related to the interaction between graphene and VO₂. Figure 3a shows that the red-shift trends of G-peak occurred as temperature increases, but only within the temperature range of 20–70 °C and diminished at higher temperature for sample A3–A6. The differences in G-peak slope from the linear fit of temperature-dependent Raman peaks data in the 20–70 °C and 20–90 °C region shown in Table 1 can confirm the diminished of red-shift trend, where sample A3–A6 show smaller slope of G-peak in the range of 20–90 °C, while the reference samples (A1–A2) have similar slopes for both temperature ranges. Generally, the G-peak position of graphene tends to red-shift linearly as temperature increases as proposed in the theoretical work by Bonini et al.²⁷, and also observed in several experimental works^{28–30}. The red-shifts of the G-peak due to temperature can be expressed as contributions from several effects³⁰:

$$\Delta\omega_G(T) = \Delta\omega_G^E(T) + \Delta\omega_G^A(T) + \Delta\omega_G^S(T) \quad (2)$$

where $\Delta\omega_G(T)$ is the frequency shift of the G-peak, $\Delta\omega_G^E(T)$ is the shift from graphene thermal expansion, which is normally positive (blue-shift) due to the negative thermal expansion nature of graphene, $\Delta\omega_G^A(T)$ is the shift due to the self-energy shift from the 4-phonon interaction, which is the intrinsic effect in graphene²⁷ and $\Delta\omega_G^S(T)$ is the shift due to the thermal expansion coefficient mismatch between graphene and its substrate. However, the observed phenomenon in this work is different. In addition to the diminished red-shift trend of G-peak, the splitting of G-peak was also observed as the temperature reached ~60 °C for both CVD graphene

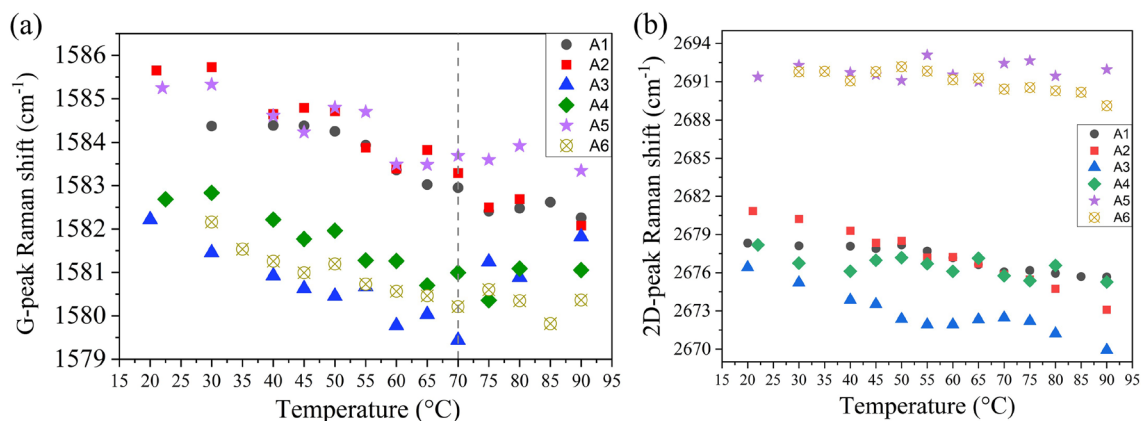


Figure 3. (a) Temperature-dependent G-Peak position of graphene on all samples (b) Temperature-dependent 2D-peak position of graphene on all samples.

Sample	G-peak (20–70 °C)	G-peak (20–90 °C)	2D-peak (20–70 °C)	2D-peak (20–90 °C)
A1: CVD graphene	-0.04270	-0.04332	-0.04052	-0.04583
A2: Exf. graphene	-0.05262	-0.05635	-0.10135	-0.10989
A3: CVD graphene/100 nm VO ₂	-0.05036	-0.01061	-0.08842	-0.07852
A4: CVD graphene/50 nm VO ₂	-0.04483	-0.03345	-0.02709	-0.02914
A5: Exf. graphene/100 nm VO ₂	-0.03883	-0.03023	0.00455	0.00482
A6: Exf. graphene/50 nm VO ₂	-0.04223	-0.02903	-0.02295	-0.03875

Table 1. Slope of temperature-dependent Raman measurement on G and 2D peaks from all samples in $\text{cm}^{-1} \text{ } ^\circ\text{C}^{-1}$.

and exfoliated graphene on VO₂ (100 nm) samples (A3-CVD/100 and A5-exf./100). The contour of Raman spectra of G-peak at various temperatures for sample A5 (exf./100) can be seen in Fig. 4a. The evolution of G-peak with temperature can be seen in Fig. 4b, as it was heated up (40–90 °C) then cooled down. The splitting occurred from G-peak at $\sim 1583 \text{ cm}^{-1}$ into G⁻ around 1580 cm^{-1} and G⁺ around 1593 cm^{-1} . The splitting disappeared after the sample was cooled down, indicating that this is a reversible process that originated from the presence of VO₂. As for the CVD graphene sample, the G-peak splitting was also observed with some different details, as shown in Fig. S5 in the supplementary file. One possible explanation for this phenomenon is the asymmetric tensile strain applied to graphene induced by the phase transition of VO₂ and its thermal expansion mismatch. The α of VO₂ for in-plane direction were calculated by Théry et al.²⁵ which are $\alpha_a^M = 12.1 \times 10^{-6} \text{ K}^{-1}$, $\alpha_c^M = 2.57 \times 10^{-6} \text{ K}^{-1}$, $\alpha_b^R = 5.83 \times 10^{-6} \text{ K}^{-1}$ and $\alpha_c^R = 29.7 \times 10^{-6} \text{ K}^{-1}$. Where the superscripts M and R indicate the monoclinic and rutile phases of VO₂, and subscripts a, b, and c indicate the direction of the crystal. In terms of direction, α_a^M is equivalent to α_c^R and α_c^M is equivalent to α_b^R . According to the theory proposed by Klimov et al.³¹, as the temperature increases, each grain of VO₂ starts to change its phase from monoclinic to rutile. The phase transition for each grain may occur at temperature before or after reaching T_{MIT} depending on their grain size³¹. The C-AFM measurement results from sample A3 (CVD/100) (see Fig. 1e,f) show that the grain boundaries are varied for both graphene/VO₂ and pure VO₂ area. Combining with the fact that the α in each in-plane direction of VO₂ are different, which α_c^R is significantly higher than the α_b^R . Therefore, it is most likely that the in-plane tensile strain from VO₂ at higher temperature tends to be asymmetric, resulting in the blue-shift of G-phonon mode in the direction with lesser tensile strain and red-shift in the higher tensile strain direction. The results presented are in good agreement with the work from Mohiuddin et al.³² which reports about the G-peak splitting due to uniaxial strain applied to the graphene on a flexible substrate.

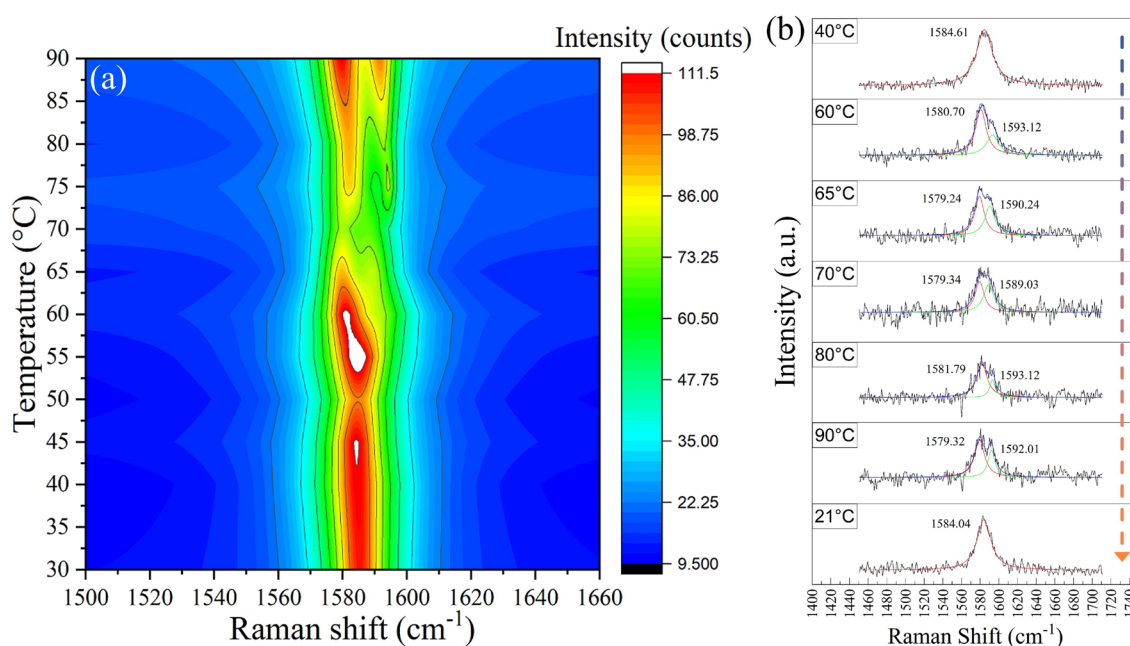


Figure 4. (a) Contour plot of graphene Raman shift from sample A5 (exf./100), the G-peak splitting starts showing at 60 °C (b) The evolution of G-peak splitting on sample A5 (exf./100) as temperature increases from 40 to 90 °C. As the sample was cooled down to 21 °C, the G-peak splitting disappeared, which can be considered as a reversible process.

Aside from the G-peak shifts, the 2D-peak measurement also yields interesting results (see Fig. 3b) The 2D-peak positions of samples A1–A4 are located in the range of 2669–2680 cm^{-1} while A5 (exf./100) and A6 (exf./50) are located between 2689 and 2693 cm^{-1} (blue-shifted by $\sim 13 \text{ cm}^{-1}$ compared to ref. sample). Normally, the 2D-peak of graphene exhibits a red-shift trend, with an even lesser slope compared to G-peak red shift trend under increasing temperature and uniaxial-strain.^{30,32} However, in contrast to our G-peak result, the temperature-dependent 2D-peak trends observed from all samples except A3 (CVD/100) are almost constant with small fluctuations instead of red-shift as observed from the reference samples A1 (CVD ref) and A2 (exf. ref) as seen in Fig. 3b and Table 1. There should be more interaction between graphene and VO₂ that modifies the electronic band structure of graphene, resulting in some modification of the double resonance Raman scattering process across the K-point of electronic dispersion, which is the origin of the 2D-peak^{29,33,34}. Further experimental and theoretical studies are required to provide further analysis.

Temperature-dependent Raman spectra of VO₂ vibrational modes were also measured and compared on sample A3–A6 on both graphene/VO₂ and pure VO₂ areas. Three main vibrational modes Raman shifts of VO₂, ~ 195 , ~ 225 and $\sim 616 \text{ cm}^{-1}$ mode, were plotted against temperature as shown in Fig. S4 in supplementary material. The trend lines between each sample are different from each other, but the trend lines observed from the same sample are almost identical except at temperatures higher than 65 °C where their Raman spectra might be too noisy (VO₂ intensity drop sharply at 65–70 °C). The similarity between the results from graphene/VO₂ area and pure-VO₂ area observed from sample A3–A6 as shown in Fig. S3 indicates that graphene layer might have no effect on VO₂ structural properties. Figure 5 shows the temperature-dependent normalized VO₂ $\sim 616 \text{ cm}^{-1}$ Raman intensity for sample A3–A6 in the heating cycle. In general, the structural phase transition curve remains almost unchanged or slightly shifts to the left, indicating that the graphene layer provides almost no effect on T_{SPT}. However, there might be a slight decrease in T_{SPT} for the thicker VO₂ (samples A3 and A5 as seen in Fig. 5a,c, respectively). The reason is that the 100 nm VO₂ is more relaxed from the substrate clamping effect compared to the 50 nm, hence the presence of graphene on top has more effect¹⁰. Therefore, the increase in T_{MIT} as discussed earlier may not originate from structural changes in VO₂. The increase in T_{MIT} is likely to originate from other factors such as the different thermal conductivity between two layers and the phase transition mechanism of VO₂ as discussed in the previous section.

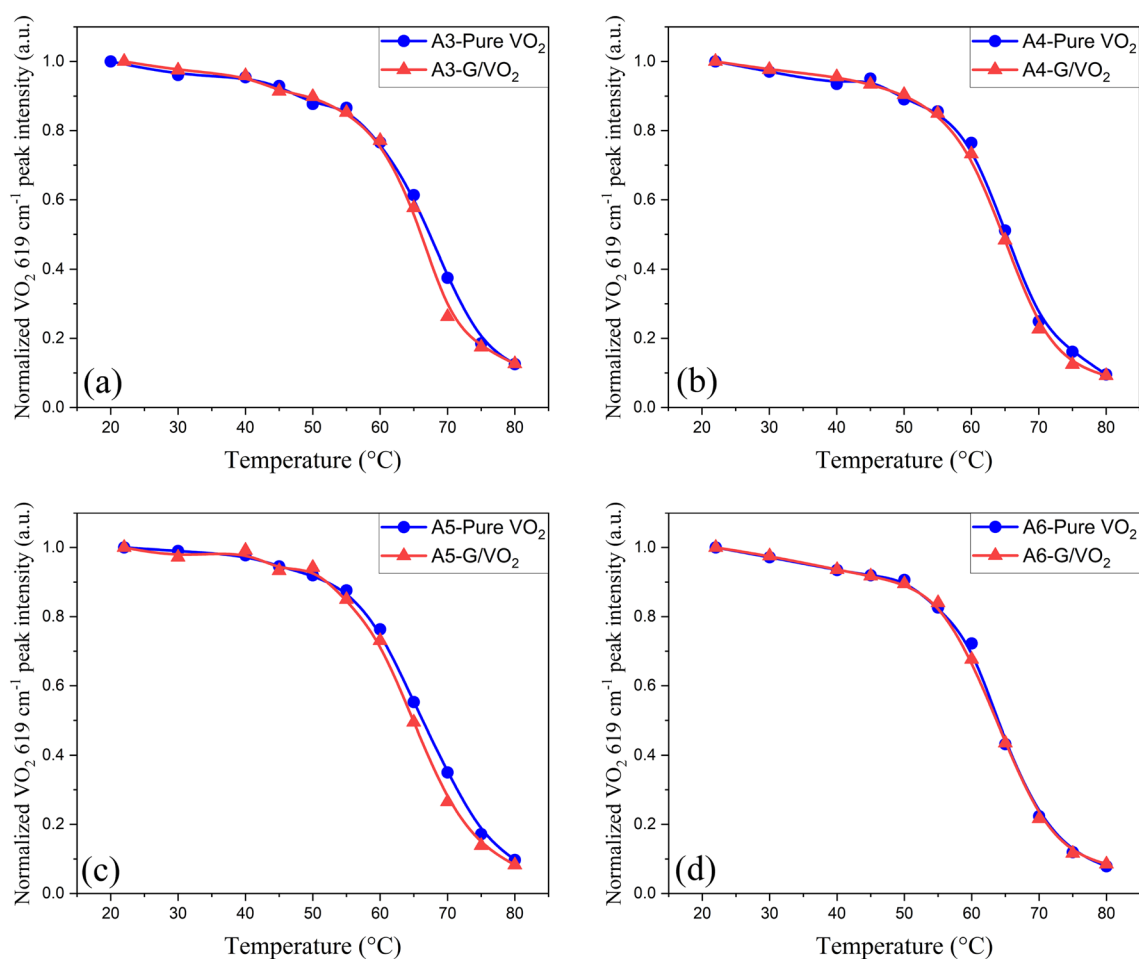


Figure 5. Temperature-dependent normalized VO₂ 616 cm^{-1} Raman intensity from sample (a) A3 (CVD/100) (b) A4 (CVD/50) (c) A5(exf./100) and (d) A6 (exf./50).

Conclusion

In order to understand the interaction between graphene and VO₂, temperature-dependent resistivity and Raman measurements were performed on graphene/VO₂/c-Al₂O₃. The samples were prepared by fabricating VO₂ using the RBTIBD technique, followed by wet transfer (for CVD graphene) or mechanical exfoliate (for exfoliated graphene) the graphene layer onto VO₂ layer. In contrast to other previous work^{15,16,35}, our samples layer ordering were swapped to graphene layer on top of VO₂ in order to study the heterostructure without worsening graphene and VO₂ layer along with minimizing the strain effect induced by lattice mismatch between graphene and VO₂. From the resistivity measurement, the less sharp phase transition characteristics and higher T_{MIT} of VO₂ on graphene/VO₂ area compared to pure VO₂ area were observed. The T_{MIT} in graphene/VO₂ samples slightly increase by ~ 1.9 °C and ~ 3.8 °C compared to pure VO₂ for sample with 100 nm and 50 nm VO₂, respectively. This might originate from a large difference between the thermal conductivity of graphene and VO₂, resulting in the graphene layer act as a heat sink, thus the VO₂ layer requires slightly higher temperature than T_{MIT} to change its phase. The effects of VO₂ phase transition on the graphene layer were observed, as seen in the G-peak splitting from temperature-dependent Raman measurements for the first time. The G-peak splitting is attributed to the asymmetric strain applied to graphene due to the thermal expansion mismatch between graphene and VO₂ during the VO₂ phase transition. The asymmetric strain may originate from the fact that each grain of VO₂ starts to change its phase at different temperatures. Thus, the strain from the thermal expansion of VO₂ can affect graphene in random direction and cause asymmetric changes of graphene structure. The 2D-peak Raman measurement results also show a large blue-shift of about 13 cm⁻¹ for exfoliated graphene on VO₂ and the absence of red-shift trends in all graphene/VO₂ samples except for sample A3 (CVD/100). There should be more electronic band interaction between graphene and VO₂ that requires further experiment to clarify. These findings may provide a better understanding of the heterostructure and introduce some possibilities for the application of graphene/VO₂ which utilizes the controllable structural properties of graphene with the help of VO₂ phase transition.

Methods

Two VO₂ thin films were deposited on top of c-Al₂O₃ substrates using the RBTIBD method. The deposition process and conditions can be found elsewhere.³⁶ The estimated thickness of the VO₂ layers measured by X-ray Reflectivity (XRR) technique are ~ 50 nm and ~ 100 nm. The surface morphology of the films and crystal structure were analyzed via AFM, XRD and Raman spectroscopy techniques. The graphene layers were transferred onto VO₂/c-Al₂O₃ and c-Al₂O₃ reference substrates using two methods: mechanical exfoliation via the scotch-tape method and the CVD graphene wet-transfer method. The first technique was performed with a natural graphite flake by spreading a few layers of graphene across a scotch-tape, then press them on the VO₂ layer. The exfoliation steps are slightly modified from Huang et al.³⁷ The latter method was performed with CVD graphene bought from Graphenea by submerging graphene and the PMMA layer into DI water to separate the graphene/sacrificial layer from the PMMA. Then, the VO₂/c-Al₂O₃ samples were dipped and fished up the graphene layer, followed by heating treatment and acetone cleaning. More detail on both transfer methods can be found in the supplementary material. The characteristics related to the phase transition of VO₂ were analyzed using the temperature-dependent Raman spectroscopy technique with a 532 nm excitation laser wavelength. The excitation laser power in this work is less than ~ 0.5 mW in order to avoid heat damage on graphene and VO₂. The grating for Raman measurement is 1800 lines/mm. Raman peaks captured from the temperature-dependent Raman results were fitted with the Lorentzian function. As for the temperature-dependent resistivity measurement, the 100 nm-thick Au electrodes were fabricated on VO₂ samples with CVD-graphene using UV-lithography and metal evaporation techniques. The measurements were conducted to probe the electrical properties of the Graphene(CVD)/VO₂ heterostructure. The temperatures were measured on mini-hot plate via thermocouple with temperature error of ± 1 °C.

Data availability

The datasets used and/or analysed during the current study available from the corresponding author on reasonable request.

Received: 4 January 2024; Accepted: 17 February 2024

Published online: 24 February 2024

References

- Morin, F. J. Oxides which show a metal-to-insulator transition at the neel temperature. *Phys. Rev. Lett.* **3**, 34–36. <https://doi.org/10.1103/PhysRevLett.3.34> (1959).
- Mott, N. F. & Friedman, L. Metal-insulator transitions in VO₂, Ti₂O₃ and Ti_{2-x}V_xO₃. *Philos. Mag. J. Theor. Exp. Appl. Phys.* **30**, 389–402. <https://doi.org/10.1080/14786439808206565> (1974).
- Shao, Z., Cao, X., Luo, H. & Jin, P. Recent progress in the phase-transition mechanism and modulation of vanadium dioxide materials. *NPG Asia Mater.* **10**, 581–605. <https://doi.org/10.1038/s41427-018-0061-2> (2018).
- Guo, X. et al. Effect of microplate size on the semiconductor-metal transition in VO₂ thin films. *New J. Chem.* **46**, 7497–7502. <https://doi.org/10.1039/D2NJ01324J> (2022).
- Babulanam, S., Eriksson, T., Niklasson, G. & Granqvist, C. Thermochromic VO₂ films for energy-efficient windows. *Solar Energy Mater.* **16**, 347–363. [https://doi.org/10.1016/0165-1633\(87\)90029-3](https://doi.org/10.1016/0165-1633(87)90029-3) (1987).
- Crunteanu, A. et al. Voltage- and current-activated metal-insulator transition in VO₂-based electrical switches: a lifetime operation analysis. *Sci. Technol. Adv. Mater.* **11**, 065002. <https://doi.org/10.1088/1468-6996/11/6/065002> (2010).
- Zhou, Y. et al. Voltage-triggered ultrafast phase transition in vanadium dioxide switches. *IEEE Electron. Device Lett.* **34**, 220–222. <https://doi.org/10.1109/LED.2012.2229457> (2013).

8. Guo, X. *et al.* High quality VO₂ thin films synthesized from V₂O₅ powder for sensitive near-infrared detection. *Sci. Rep.* <https://doi.org/10.1038/s41598-021-01025-8> (2021).
9. Guo, X. *et al.* Synthesis, metal-insulator transition, and photoresponse characteristics of VO₂ nanobeams via an oxygen inhibitor-assisted vapor transport method. *J. Mater. Chem. C* **11**, 5731–5739. <https://doi.org/10.1039/D2TC05295D> (2023).
10. Kittiwatanakul, S., Wolf, S. A. & Lu, J. Large epitaxial bi-axial strain induces a Mott-like phase transition in VO₂. *Appl. Phys. Lett.* **105**, 073112. <https://doi.org/10.1063/1.4893326> (2014).
11. Cui, J., Jiang, Q., Wang, N. & Liang, S. Regulating the phase transition temperature of VO₂ films via the combination of doping and strain methods. *AIP Adv.* **13**, 055316. <https://doi.org/10.1063/5.0138303> (2023).
12. Shen, N. *et al.* Phase transition hysteresis of tungsten doped VO₂ synergistically boosts the function of smart windows in ambient conditions. *ACS Appl. Electron. Mater.* **3**, 3648–3656. <https://doi.org/10.1021/acsaem.1c00550> (2021).
13. Bae, S., Kim, H. & Lee, Y. E. A. Roll-to-roll production of 30-inch graphene films for transparent electrodes. *Nat. Nanotech.* **5**, 574–578. <https://doi.org/10.1038/nnano.2010.132> (2010).
14. Bolotin, K. *et al.* Ultrahigh electron mobility in suspended graphene. *Solid State Commun.* **146**, 351–355. <https://doi.org/10.1016/j.ssc.2008.02.024> (2008).
15. Kim, H. *et al.* Enhanced optical response of hybridized VO₂/graphene films. *Nanoscale* **5**, 2632–2636. <https://doi.org/10.1039/C3NR34054F> (2013).
16. Zhou, H. *et al.* Electron transfer induced thermochromism in a VO₂-graphene-Ge heterostructure. *J. Mater. Chem. C* **3**, 5089–5097. <https://doi.org/10.1039/C5TC00448A> (2015).
17. Kim, H. *et al.* Flexible thermochromic window based on hybridized VO₂/graphene. *ACS Nano* **7**, 5769–5776. <https://doi.org/10.1021/nn400358x> (2013).
18. Yu, X. *et al.* Graphene-assisting nonvolatile vanadium dioxide phase transition for neuromorphic machine vision. *Adv. Funct. Mater.* <https://doi.org/10.1002/adfm.202312481> (2024).
19. Chen, W. *et al.* A dual ultra-broadband switchable high-performance terahertz absorber based on hybrid graphene and vanadium dioxide. *Phys. Chem. Chem. Phys.* **25**, 20414–20421. <https://doi.org/10.1039/D3CP01312J> (2023).
20. Lim, S., Park, H., Yamamoto, G., Lee, C. & Suk, J. W. Measurements of the electrical conductivity of monolayer graphene flakes using conductive atomic force microscopy. *Nanomaterials* <https://doi.org/10.3390/nano11102575> (2021).
21. Muraoka, Y., Ueda, Y. & Hiroi, Z. Large modification of the metal-insulator transition temperature in strained VO₂ films grown on TiO₂ substrates. *J. Phys. Chem. Solids* **63**, 965–967. [https://doi.org/10.1016/S0022-3697\(02\)00098-7](https://doi.org/10.1016/S0022-3697(02)00098-7) (2002).
22. Mann, S., Kumar, R. & Jindal, V. K. Negative thermal expansion of pure and doped graphene. *RSC Adv.* **7**, 22378–22387. <https://doi.org/10.1039/C7RA01591G> (2017).
23. Kim, H. G. *et al.* Effect of graphene-substrate conformity on the in-plane thermal conductivity of supported graphene. *Carbon* **125**, 39–48. <https://doi.org/10.1016/j.carbon.2017.09.033> (2017).
24. Oh, D.-W., Ko, C., Ramanathan, S. & Cahill, D. G. Thermal conductivity and dynamic heat capacity across the metal-insulator transition in thin film VO₂. *Appl. Phys. Lett.* **96**, 151906. <https://doi.org/10.1063/1.3394016> (2010).
25. Théry, V. *et al.* Role of thermal strain in the metal-insulator and structural phase transition of epitaxial VO₂ films. *Phys. Rev. B* **93**, 184106. <https://doi.org/10.1103/PhysRevB.93.184106> (2016).
26. Ferrari, A. C. *et al.* Raman spectrum of graphene and graphene layers. *Phys. Rev. Lett.* **97**, 187401. <https://doi.org/10.1103/PhysRevLett.97.187401> (2006).
27. Bonini, N., Lazzeri, M., Marzari, N. & Mauri, F. Phonon anharmonicities in graphite and graphene. *Phys. Rev. Lett.* **99**, 176802. <https://doi.org/10.1103/PhysRevLett.99.176802> (2007).
28. Calizo, I., Balandin, A. A., Bao, W., Miao, F. & Lau, C. N. Temperature dependence of the Raman spectra of graphene and graphene multilayers. *Nano Lett.* **7**, 2645–2649. <https://doi.org/10.1021/nl071033g> (2007).
29. Late, D. J., Maitra, U., Panchakarla, L. S., Waghmare, U. V. & Rao, C. N. R. Temperature effects on the Raman spectra of graphenes: Dependence on the number of layers and doping. *J. Phys. Condens. Matter* **23**, 055303. <https://doi.org/10.1088/0953-8984/23/5/055303> (2011).
30. Wang, W., Peng, Q., Dai, Y., Qian, Z. & Liu, S. Temperature dependence of Raman spectra of graphene on copper foil substrate. *J. Mater. Sci.: Mater. Electron.* **27**, 3888–3893. <https://doi.org/10.1007/s10854-015-4238-y> (2016).
31. Klimov, V. *et al.* Hysteresis loop construction for the metal-semiconductor phase transition in vanadium dioxide films. *Tech. Phys.* **47**, 1134–1139. <https://doi.org/10.1134/1.1508078> (2002).
32. Mohiuddin, T. M. G. *et al.* Uniaxial strain in graphene by Raman spectroscopy: *g* peak splitting, Grüneisen parameters, and sample orientation. *Phys. Rev. B* **79**, 205433. <https://doi.org/10.1103/PhysRevB.79.205433> (2009).
33. Narula, R. & Reich, S. Double resonant Raman spectra in graphene and graphite: A two-dimensional explanation of the Raman amplitude. *Phys. Rev. B* **78**, 165422. <https://doi.org/10.1103/PhysRevB.78.165422> (2008).
34. Ferralis, N. Probing mechanical properties of graphene with Raman spectroscopy. *J. Mater. Sci.* **45**, 5135–5149. <https://doi.org/10.1007/s10853-010-4673-3> (2010).
35. Cao, H. *et al.* Enhancing the metal-insulator transition in VO₂ heterostructures with graphene interlayers. *Appl. Phys. Lett.* **121**, 081601. <https://doi.org/10.1063/5.0100493> (2022).
36. Kittiwatanakul, S. *et al.* Transport behavior and electronic structure of phase pure VO₂ thin films grown on c-plane sapphire under different O₂ partial pressure. *J. Appl. Phys.* **114**, 053703. <https://doi.org/10.1063/1.4817174> (2013).
37. Huang, Y. *et al.* Reliable exfoliation of large-area high-quality flakes of graphene and other two-dimensional materials. *ACS Nano* **9**, 10612–10620. <https://doi.org/10.1021/acsnano.5b04258> (2015).

Acknowledgements

The authors would like to express gratitude to M. Liu from Stony Brook University for the advice and discussion on conductive atomic force microscopy technique and S.A. Wolf from University of Virginia for the support on deposition system. Raman spectroscopy measurement has been partially provided by the funding from Thailand Science Research and Innovation Fund Chulalongkorn University. K.L. and S.K. acknowledge the support from the Second Century Fund (C2F), Chulalongkorn University; Office of the Permanent Secretary, Ministry of Higher Education, Science, Research and Innovation: Research Grant for New Scholar (RGNS) through the Grant No. RGNS 63-018 and the NSRF via the Program Management Unit for Human Resources & Institutional Development, Research and Innovation [Grant No. B37G660011].

Author contributions

K.L. designed and conducted all the experiments, analysed the results and prepared manuscript. W.R. reviewed literature and conducted experiments in early phase. I.K. and T.T. assisted on graphene exfoliation and results discussion. T.P., T.B., T.T., P.K., L.S., C.S. and S.C. provided instruments and resource supports. S.K. designed temperature-dependent resistivity experiment, analysed the results and reviewed manuscript.

Competing interests

The authors declare no competing interests

Additional information

Supplementary Information The online version contains supplementary material available at <https://doi.org/10.1038/s41598-024-54844-w>.

Correspondence and requests for materials should be addressed to S.K.

Reprints and permissions information is available at www.nature.com/reprints.

Publisher's note Springer Nature remains neutral with regard to jurisdictional claims in published maps and institutional affiliations.



Open Access This article is licensed under a Creative Commons Attribution 4.0 International License, which permits use, sharing, adaptation, distribution and reproduction in any medium or format, as long as you give appropriate credit to the original author(s) and the source, provide a link to the Creative Commons licence, and indicate if changes were made. The images or other third party material in this article are included in the article's Creative Commons licence, unless indicated otherwise in a credit line to the material. If material is not included in the article's Creative Commons licence and your intended use is not permitted by statutory regulation or exceeds the permitted use, you will need to obtain permission directly from the copyright holder. To view a copy of this licence, visit <http://creativecommons.org/licenses/by/4.0/>.

© The Author(s) 2024